References

1. Dong JF. Structural and functional correlation of ADAMTS13. Curr Opin Hematol. 2007;14:270-276.

2. Bergmeier W, Chauhan AK, Wagner DD. Glycoprotein Ibalpha and von Willebrand factor in primary platelet adhesion and thrombus formation: lessons from mutant mice. Thromb Haemost. 2008;99:264-270.

3. Tsai HM. Thrombotic thrombocytopenic purpura: a thrombotic disorder caused by ADAMTS13 deficiency. Hematol Oncol Clin North Am. 2007;21:609-632.

4. Zheng XL, Sadler JE. Pathogenesis of thrombotic microangiopathies. Annu Rev Pathol. 2008;3:249-277.

5. Desch KC, Motto DG. Thrombotic thrombocytopenic purpura in humans and mice. Arterioscler Thromb Vasc Biol. 2007;27:1901-1908.

6. Soejima K, Matsumoto M, Kokame K, et al. ADAMTS-13 cysteine-rich/spacer domains are functionally essential for von Willebrand factor cleavage. Blood. 2003;102:3232-3237.

7. Zheng X, Nishio K, Majerus EM, Sadler JE. Cleavage of von Willebrand factor requires the spacer domain of the metalloprotease ADAMTS13. J Biol Chem. 2003;278:30136-30141.

8. Ai J, Smith P, Wang S, Zhang P, Zheng XL. The proximal carboxyl-terminal domains of ADAMTS13 determine substrate specificity and are all required for cleavage of von Willebrand factor. J Biol Chem. 2005;280:29428-29434.

9. Majerus EM, Anderson PJ, Sadler JE. Binding of ADAMTS13 to von Willebrand

factor. J Biol Chem. 2005;280:21773-21778.

10. Tao Z, Wang Y, Choi H, et al. Cleavage of ultralarge multimers of von Willebrand factor by C-terminal-truncated mutants of ADAMTS-13 under flow. Blood. 2005;106:141-143.

11. Tao Z, Peng Y, Nolasco L, et al. Recombinant CUB-1 domain polypeptide inhibits the cleavage of ULVWF strings by ADAMTS13 under flow conditions. Blood. 2005;106:4139-4145.

12. Gao W, Anderson PJ, Majerus EM, Tuley EA, Sadler JE. Exosite interactions contribute to tension-induced cleavage of von Willebrand factor by the antithrombotic ADAMTS13 metalloprotease. Proc Natl Acad Sci U S A. 2006;103:19099-19104.

13. Zhang P, Pan W, Rux AH, Sachais BS, Zheng XL. The cooperative activity between the carboxyl-terminal TSP1 repeats and the CUB domains of ADAMTS13 is crucial for recognition of von Willebrand factor under flow. Blood. 2007;110:1887-1894.

14. Banno F, Kaminaka K, Soejima K, Kokame K, Miyata T. Identification of strain-specific variants of mouse Adamts13 gene encoding von Willebrand factor-cleaving protease. J Biol Chem. 2004;279:30896-30903.

15. Zhou W, Bouhassira EE, Tsai HM. An IAP retrotransposon in the mouse ADAMTS13 gene creates ADAMTS13 variant proteins that are less effective in cleaving von Willebrand factor multimers. Blood. 2007;110:886-893.

16. Banno F, Miyata T. Biology of an antithrombotic factor-ADAMTS13. In: Tanaka K, Davie EW, eds. Resent Advances in Thrombosis and Hemostasis 2008: Springer; 2008:162-176.

17. Banno F, Kokame K, Okuda T, et al. Complete deficiency in ADAMTS13 is prothrombotic, but it alone is not sufficient to cause thrombotic thrombocytopenic purpura.

Blood. 2006;107:3161-3166.

18. Miyata T, Kokame K, Banno F, Shin Y, Akiyama M. ADAMTS13 assays and ADAMTS13-deficient mice. Curr Opin Hematol. 2007;14:277-283.

19. Kokame K, Matsumoto M, Fujimura Y, Miyata T. VWF73, a region from D1596 to R1668 of von Willebrand factor, provides a minimal substrate for ADAMTS-13. Blood. 2004;103:607-612.

20. Kokame K, Nobe Y, Kokubo Y, Okayama A, Miyata T. FRETS-VWF73, a first fluorogenic substrate for ADAMTS13 assay. Br J Haematol. 2005;129:93-100.

21. Tsuji S, Sugimoto M, Miyata S, Kuwahara M, Kinoshita S, Yoshioka A. Real-time analysis of mural thrombus formation in various platelet aggregation disorders: distinct shear-dependent roles of platelet receptors and adhesive proteins under flow. Blood. 1999;94:968-975.

22. Chauhan AK, Motto DG, Lamb CB, et al. Systemic antithrombotic effects of ADAMTS13. J Exp Med. 2006;203:767-776.

23. Ni H, Denis CV, Subbarao S, et al. Persistence of platelet thrombus formation in arterioles of mice lacking both von Willebrand factor and fibrinogen. J Clin Invest. 2000;106:385-392.

24. Frenette PS, Moyna C, Hartwell DW, Lowe JB, Hynes RO, Wagner DD. Platelet-endothelial interactions in inflamed mesenteric venules. Blood. 1998;91:1318-1324.

25. DiMinno G, Silver MJ. Mouse antithrombotic assay: a simple method for the evaluation of antithrombotic agents in vivo. Potentiation of antithrombotic activity by ethyl alcohol. J Pharmacol Exp Ther. 1983;225:57-60.

26. Jackson SP. The growing complexity of platelet aggregation. Blood.

2007;109:5087-5095.

27. Konstantinides S, Ware J, Marchese P, Almus-Jacobs F, Loskutoff DJ, Ruggeri ZM. Distinct antithrombotic consequences of platelet glycoprotein Ibalpha and VI deficiency in a mouse model of arterial thrombosis. J Thromb Haemost. 2006;4:2014-2021.

28. Shida Y, Nishio K, Sugimoto M, et al. Functional imaging of shear-dependent activity of ADAMTS13 in regulating mural thrombus growth under whole blood flow conditions. Blood. 2008;111:1295-1298.

29. Smyth SS, Reis ED, Vaananen H, Zhang W, Coller BS. Variable protection of beta 3-integrin--deficient mice from thrombosis initiated by different mechanisms. Blood. 2001;98:1055-1062.

30. Cui J, Eitzman DT, Westrick RJ, et al. Spontaneous thrombosis in mice carrying the factor V Leiden mutation. Blood. 2000;96:4222-4226.

31. Weiler H, Lindner V, Kerlin B, et al. Characterization of a mouse model for thrombomodulin deficiency. Arterioscler Thromb Vasc Biol. 2001;21:1531-1537.

32. Suh TT, Holmback K, Jensen NJ, et al. Resolution of spontaneous bleeding events but failure of pregnancy in fibrinogen-deficient mice. Genes Dev. 1995;9:2020-2033.

33. Toomey JR, Kratzer KE, Lasky NM, Broze GJ, Jr. Effect of tissue factor deficiency on mouse and tumor development. Proc Natl Acad Sci U S A. 1997;94:6922-6926.

34. Motto DG, Chauhan AK, Zhu G, et al. Shigatoxin triggers thrombotic thrombocytopenic purpura in genetically susceptible ADAMTS13-deficient mice. J Clin Invest. 2005;115:2752-2761.

35. Nishio K, Anderson PJ, Zheng XL, Sadler JE. Binding of platelet glycoprotein Ibalpha to von Willebrand factor domain A1 stimulates the cleavage of the adjacent domain A2

by ADAMTS13. Proc Natl Acad Sci U S A. 2004;101:10578-10583.

36. Shim K, Anderson PJ, Tuley EA, Wiswall E, Sadler JE. Platelet-VWF complexes are preferred substrates of ADAMTS13 under fluid shear stress. Blood. 2008;111:651-657.

37. Donadelli R, Orje JN, Capoferri C, Remuzzi G, Ruggeri ZM. Size regulation of von Willebrand factor-mediated platelet thrombi by ADAMTS13 in flowing blood. Blood. 2006;107:1943-1950.

38. Chauhan AK, Walsh MT, Zhu G, Ginsburg D, Wagner DD, Motto DG. The combined roles of ADAMTS13 and VWF in murine models of TTP, endotoxemia, and thrombosis. Blood. 2008;111:3452-3457.

Figure Legends

Figure 1. Generation of *Adamts13*$^{S/S}$ mice with 129/Sv-genetic background. (A) Gene and protein structure of ADAMTS13 in the wild-type (*Adamts13*$^{L/L}$) 129/Sv mice, the *Adamts13*$^{S/S}$ mice on 129/Sv genetic background, and the *Adamts13*$^{-/-}$ mice on 129/Sv genetic background. An intracisternal A-particle (*IAP*) insertion into intron 23 creates a pseudo-exon 24 including a premature stop codon. ADAMTS13 with a truncated C-terminus is mainly expressed in *Adamts13*$^{S/S}$ mice. *S*, signal peptide; *P*, propeptide; *MP*, metalloprotease domain; *Dis*, disintegrin-like domain; *T* (*numbered 1-8*), thrombospondin type 1 motif domain; *Cys*, cysteine-rich domain; *Sp*, spacer domain; *CUB*, complement components C1r/C1s, urchin epidermal growth factor, and bone morphogenic protein-1 domain. (B) Expression of *Adamts13* mRNA in liver. Poly(A)$^+$ RNA isolated from liver of indicated mice was probed with a 1.3-kb Adamts13 cDNA corresponding to exons 3-13. (C) GST-mVWF73-H assay. Plasma ADAMTS13 activity of indicated mice was measured using a recombinant mouse VWF73 peptide, GST-mVWF73-H. Results from 6 mice for each genotype are shown. Standard reactions using graded amounts of pooled plasma from 10 *Adamts13*$^{L/L}$ mice were performed simultaneously. (D) FRETS-VWF73 assay. Plasma ADAMTS13 activity in indicated mice was determined using a fluorogenic human VWF73 peptide, FRETS-VWF73. Data are mean ± SD of 6 mice for each genotype. The average activity measured in *Adamts13*$^{L/L}$ mice was arbitrarily defined as 100%.

Figure 2. Plasma VWF multimers. (A) VWF multimer patterns. Plasma samples (1 μL/lane) from *Adamts13*$^{L/L}$, *Adamts13*$^{S/S}$, and *Adamts13*$^{-/-}$ mice were electrophoresed on SDS-agarose

gels and transferred to nitrocellulose membranes. VWF multimers were detected with anti-VWF antibodies. (B) Relative intensities of plasma VWF multimers. The chemiluminescent intensities of the VWF multimer patterns (*A*) were scanned using image analysis software. An average of multiple lanes from 4 mice for each genotype are shown. *HMW*, high molecular weight; *LMW*, low molecular weight.

Figure 3. In vitro thrombogenesis on collagen surface under flow. (A) Thrombus formation at 1000 s^{-1}. Whole blood from *Adamts13*$^{L/L}$, *Adamts13*$^{S/S}$, or *Adamts13*$^{-/-}$ mice containing mepacrine-labeled platelets was perfused over an acid-insoluble type I collagen-coated surface at a wall shear rate of 1000 s^{-1}. The cumulative thrombus volume, analyzed using a multi-dimensional imaging system, was measured every 0.5 min until 4 min. Data are the mean ± SEM of 25 mice for each genotype. (B) Thrombus formation at 5000 s^{-1}. Whole blood samples from indicated mice were perfused over an acid-insoluble type I collagen-coated surface at a wall shear rate of 5000 s^{-1}. The cumulative thrombus volume was measured every 20 s until 80 s. Blood from 2 mice was pooled and used for experiments. Data are the mean ± SEM of 15 samples for each genotype. *Asterisks* indicate significant differences at $P < 0.05$ in comparison to *Adamts13*$^{L/L}$ mice.

Figure 4. In vivo thrombogenesis in ferric chloride-injured mesenteric arterioles. (A) Time to first thrombus formation. Calcein AM-labeled platelets representing approximately 2.5% of total platelets were observed in mesenteric arterioles of live mice after injury with 10% ferric chloride. The time required for formation of a thrombus > 30 μm was measured. (B) Occlusion time. The time required for a complete stop of blood flow was measured after injury

with 10% ferric chloride. *Symbols* represent data from a single mouse. *Bars* represent the mean values of groups (n = 16 for *Adamts13*$^{L/L}$ mice, n = 16 for *Adamts13*$^{S/S}$ mice and n = 12 for *Adamts13*$^{-/-}$ mice).

Figure 5. Platelet counts after collagen plus epinephrine infusion. Mice were injected with 600 ng/g of collagen plus 60 ng/g of epinephrine via tail vein and platelet counts were measured 5 min after injection. *Symbols* represent platelet counts from a single mouse. *Bars* represent the mean values of 25 mice in each group. Platelet counts of untreated mice were not different among the groups.

Figure 1

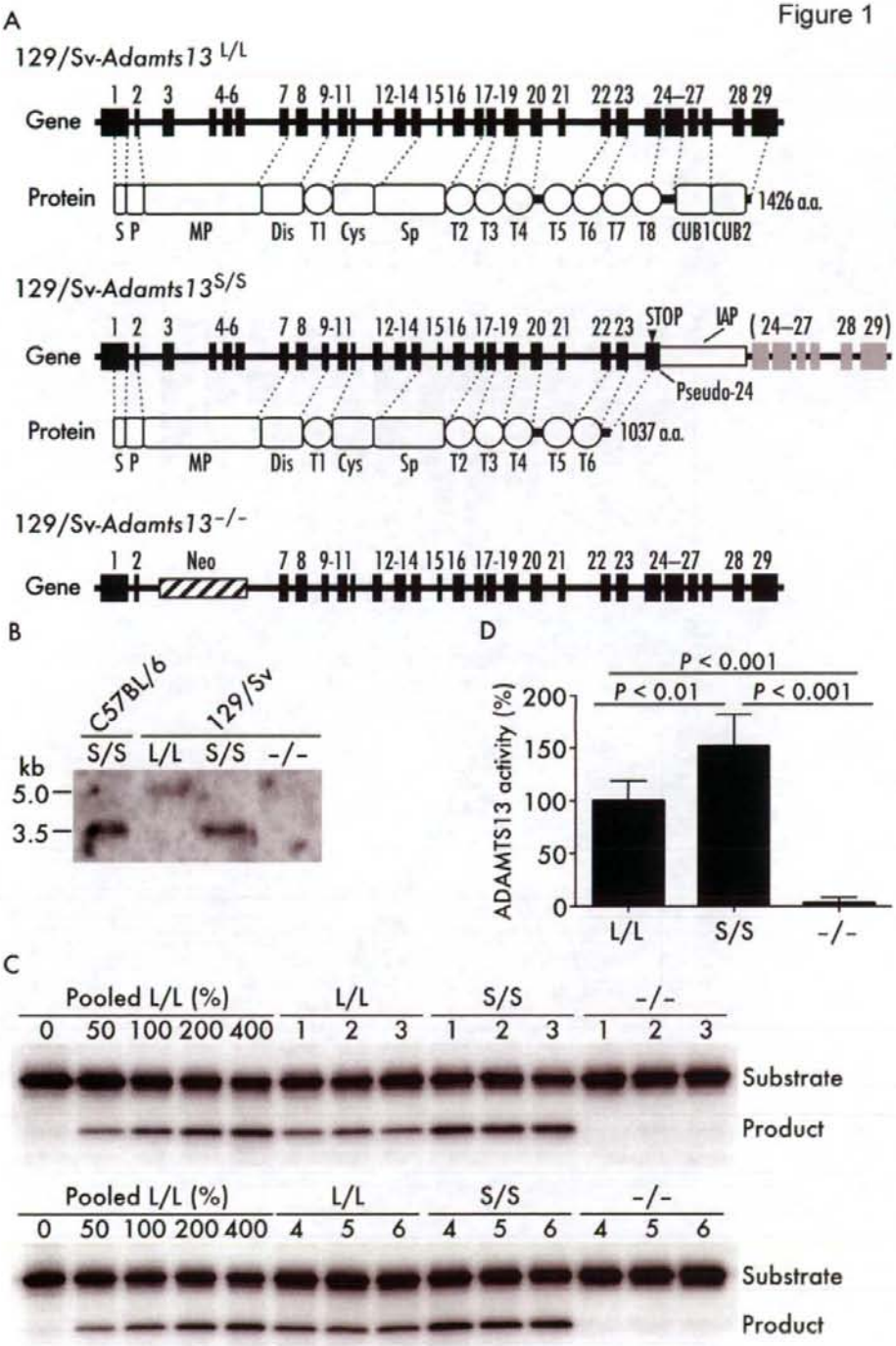
A
129/Sv-Adamts13 L/L
Gene
1 2 3 4-6 7 8 9-11 12-14 15 16 17-19 20 21 22 23 24–27 28 29
Protein
1426 a.a.
S P MP Dis T1 Cys Sp T2 T3 T4 T5 T6 T7 T8 CUB1 CUB2
129/Sv-Adamts13 S/S
Gene
1 2 3 4-6 7 8 9-11 12-14 15 16 17-19 20 21 22 23 STOP IAP (24–27 28 29)
Pseudo-24
Protein
1037 a.a.
S P MP Dis T1 Cys Sp T2 T3 T4 T5 T6
129/Sv-Adamts13 -/-
Gene
1 2 Neo 7 8 9-11 12-14 15 16 17-19 20 21 22 23 24–27 28 29
B
C57BL/6
129/Sv
S/S L/L S/S -/-
kb
5.0
3.5
D
P < 0.001
P < 0.01
P < 0.001
ADAMTS13 activity (%)
200
150
100
50
0
L/L
S/S
-/-
C
Pooled L/L (%)
0 50 100 200 400
L/L
1 2 3
S/S
1 2 3
-/-
1 2 3
Substrate
Product
Pooled L/L (%)
0 50 100 200 400
L/L
4 5 6
S/S
4 5 6
-/-
4 5 6
Substrate
Product

Figure 2

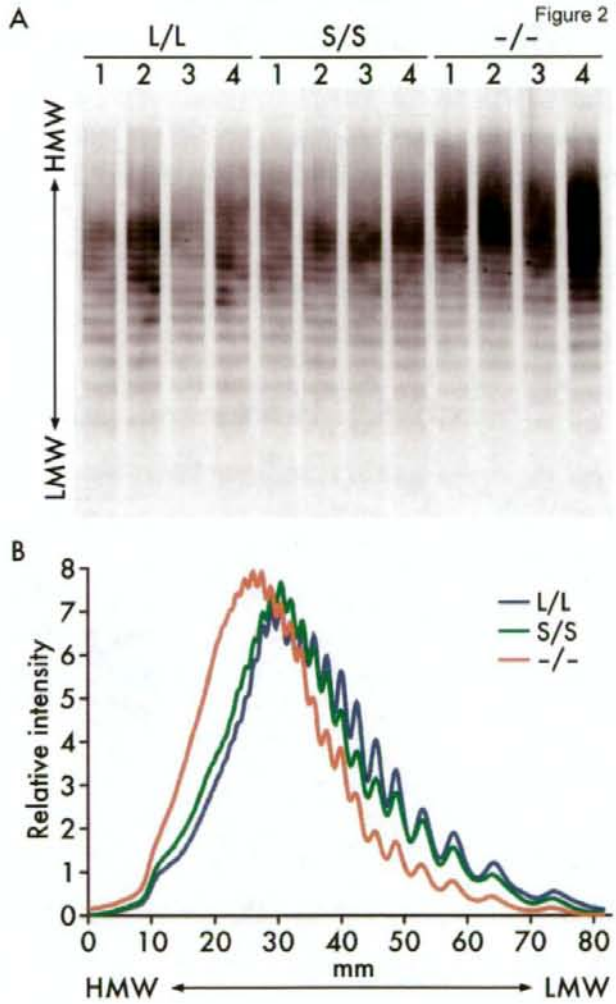
A
L/L
S/S
-/-
1 2 3 4 1 2 3 4 1 2 3 4
HMW
LMW
B
Relative intensity
0 1 2 3 4 5 6 7 8
L/L
S/S
-/-
0 10 20 30 40 50 60 70 80
mm
HMW
LMW

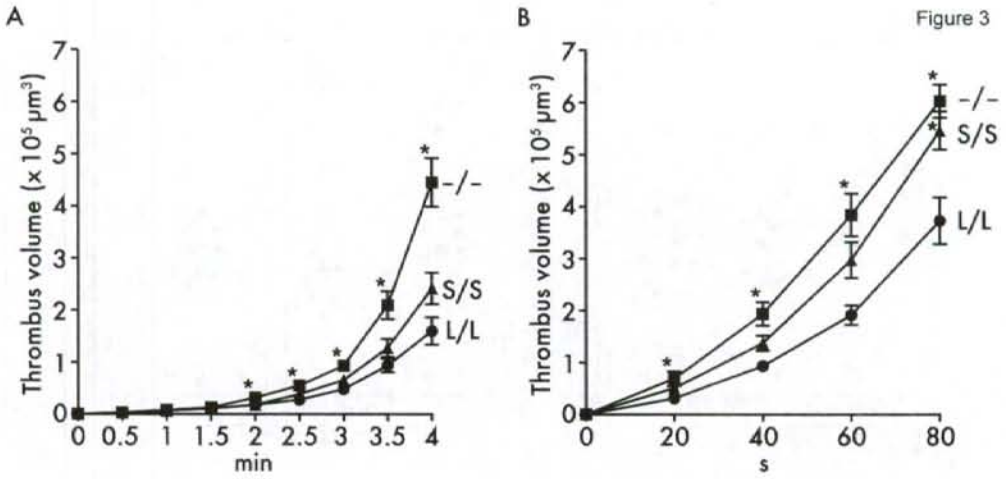
A
B
Thrombus volume (x 10⁵ µm³)
min
s
-/-
S/S
L/L
0
0.5
1
1.5
2
2.5
3
3.5
4
20
40
60
80
*

Figure 3

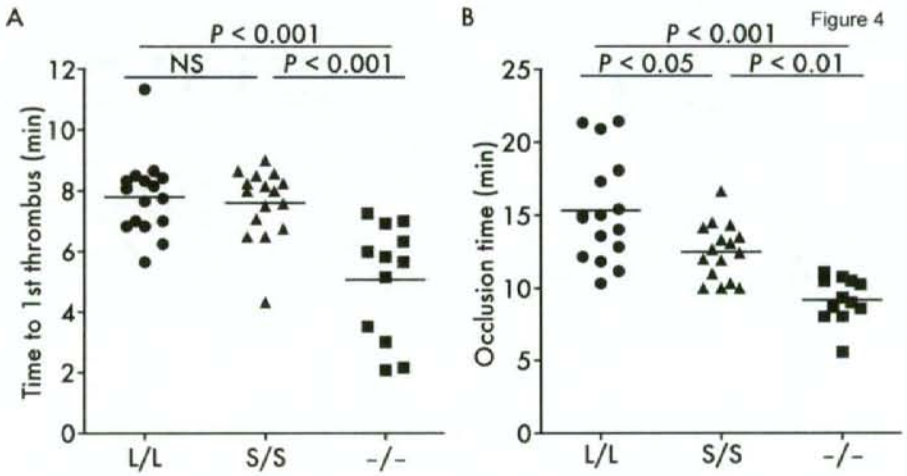
A
P < 0.001
NS
P < 0.001
Time to 1st thrombus (min)
12
10
8
6
4
2
0
L/L
S/S
-/-
B
P < 0.001
P < 0.05
P < 0.01
Occlusion time (min)
25
20
15
10
5
0
L/L
S/S
-/-

Figure 4

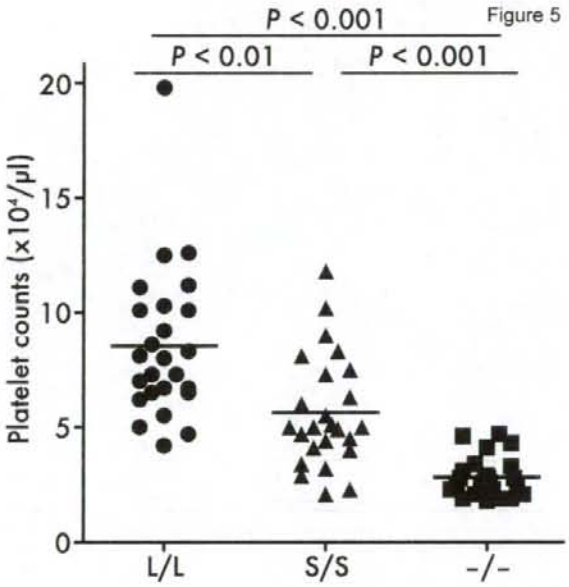

Figure 5

Exp. Anim. 57(4), 385–395, 2008

Type 2 Diabetes Mellitus in a Non-Obese Mouse Model Induced by Meg1/Grb10 *Overexpression*

Yoshie YAMAMOTO[1, 2], Fumitoshi ISHINO[3], Tomoko KANEKO-ISHINO[4], Hirosuke SHIURA[3], Kozue UCHIO-YAMADA[5], Junichiro MATSUDA[5], Osamu SUZUKI[5], and Katsunori SATO[2]

[1]Department of Veterinary Science, National Institute of Infectious Diseases, 1–23–1 Toyama, Shinjuku-ku, Tokyo 162-8640, [2]Okayama University Graduate School of Natural Science and Technology, 3–1–1 Tsushima-naka, Okayamashi, Okayama 700-8530, [3]Department of Epigenetics, Medical Research Institute, Tokyo Medical and Dental University, 1–5–45 Yushima, Bunkyou-ku, Tokyo 113-8510, [4]Tokai University School of Health Sciences, Bohseidai, Isehara, Kanagawa 259-1193, and [5]Division of Biomedical Research Resources, National Institute of Biomedical Innovation, 7–6–8 Saito-Asagi, Ibaraki, Osaka 567-0085, Japan

Abstract: *We assessed the possibility of C57BL/6-Tg (*Meg1/Grb10*)isn(Meg1 Tg) mice as a non-obese type 2 diabetes (2DM) animal model. Meg1 Tg mice were born normal, but their weight did not increase as much as normal after weaning and showed about 85% of normal size at 20 weeks of age. Body mass index of Meg1 Tg mice was also smaller than that of control mice. The glucose tolerance test and insulin tolerance test showed that Meg1 Tg mice had reduced ability to normalize the blood glucose level. Blood urea nitrogen (BUN) in Meg1 Tg mice (19.6 ± 1.2 mg/dl) was significantly lower than in controls (22.0 ± 0.8 mg/dl), while plasma triglyceride, insulin, adiponectin, and resistin levels were significantly higher (202.0 ± 23.4 mg/dl vs 146.3 ± 23.4 mg/dl, 152.4 ± 16.3 pg/ml vs 88.1 ± 16.9 pg/ml, 74.4 ± 10.9 μg/ml vs 48.3 ± 7.0 μg/ml, and 4.0 ± 0.2 ng/ml vs 3.6 ± 0.2 ng/ml, respectively). Body, visceral fat weight and liver weights were significantly lower (19.6 ± 0.4 g vs 24.3 ± 0.3 g, 376.7 ± 29.6 mg to 507.5 ± 23.0 mg, and 906.0 ± 41.8 mg to 1,001.0 ± 15.1 mg, respectively). Thus, hyperinsulinemia observed in Meg1 Tg mice indicates that their insulin signaling pathway is somehow inhibited. With high fat diet, the diabetes onset rate of Meg1 Tg mice increased up to 60%. These results suggest that Meg1 Tg mice resemble human 2DM.*

Key words: *biochemical characterization,* Meg1/Grb10 *transgenic mouse, non-obese mouse model, type 2 diabetes mellitus*

Introduction

Type 2 diabetes mellitus (2DM) is a life-threatening endocrine disorder that affects as many as 6% to 10% of the population of the world. This type of diabetes is classified as non-insulin dependent diabetes and accounts for higher than 95% of all cases of diabetes [12, 39]. Moreover, recent studies have revealed that the prevalence of 2DM has doubled in the United States over the last 30 years [1].

(Received 2 November 2007 / Accepted 24 March 2008)

Address corresponding: Y. Yamamoto, Department of Veterinary Science, National Institute of Infectious Diseases, 1–23–1 Toyama, Shinjuku-ku, Tokyo 162-8640, Japan

Many experimental 2DM model animals have been established from spontaneous mutants and are currently in use in human 2DM research [11, 22, 24, 33, 35]. In spite of much effort, which has focused on using such model animals, some aspects of 2DM remain unclear. To elucidate the pathological character of 2DM, it is necessary to identify which metabolic pathways are responsible for the onset of 2DM. However, in many cases, the relationship between original mutations and their affected metabolic pathways is difficult to explain. Recent progress in molecular biology has enabled us to take another approach to develop novel diabetes model animals through the manipulation of genes that are closely related to glucose metabolism and insulin resistance [6]. Using gene-targeting technology, a number of useful mouse models have recently been developed for the study of the progression of diabetes [4, 17].

Recently, genomic imprinting has been discovered as an important factor in the etiology of 2DM. A number of studies have reported a relationship between genomic imprinting and 2DM in the mouse [13, 21, 30]. Overexpression of some imprinted genes might explain the mechanism of human transient neonatal diabetes [21], and deletion of some imprinted genes has been suggested as the cause of pancreatic β cell dysfunction [13]. Another candidate imprinted gene for 2DM is maternally expressed 1(Meg1)/ growth factor receptor-binding protein (Grb) 10 [23]. Recently, it has been reported that *Meg1/Grb10* knockout mice show the embryonic overgrowth phenotype [3]. *Meg/Grb10* transgenic mice Meg1 Tg mice were produced to elucidate Meg1/Grb10 function *in vivo* [31]. Grb10 interacts with both insulin receptors (IR) and insulin-like growth factor I receptors (IGF-1R) *in vitro* [8, 9, 27]. Since the IGF-1 signaling pathway is reportedly involved in embryonic growth, Meg1/Grb10 may have a negative effect both on the embryonic growth and postnatal growth phenotypes associated with uniparental duplication of chromosome 11 [7, 23]. Alternatively, Meg1/Grb10 may function in glucose homeostasis, which is regulated by the IR signaling pathway. Insulin binds to IR and activates a signal transduction pathway through its receptor kinase activity. It has been demonstrated that IGF1 functions via IGF1R, while IGF2 functions via both IGF1R and IR, and that each of these signaling pathways contributes to some extent to late embryonic growth [20]. Moreover, mutation studies of human 2DM patients indicate the existence of additional factors in the pathogenesis of this disease [25].

Overall, Meg1 Tg mice have similar character to human 2DM in overexpression of the imprinted Meg1/Grb10 gene that functions negatively for both insulin signaling via IR and IGF-1 signaling via IGF-1R. Therefore, it seems likely that, in the late embryonic stage, when endogenous Meg1/Grb10 expression is very high, Meg1/Grb10 negatively regulates growth via modulation of both the IR and IGF1R cascades [31]. There are few data about biochemical changes in the Meg1 Tg mouse. To be useful in therapeutic research the model mouse has to show a similar phenotype to human 2DM. Furthermore, the incidence rate of the onset of 2DM in Meg1 Tg mice fed on basal diet was reportedly small [30].

In this study, we examined several basic biochemical characters of Meg1 Tg mice as a 2DM model, and the effects of diet on the onset of 2DM. The results indicate that the Meg1 Tg mouse is a useful non-obese 2DM mouse model.

Materials and Methods

Animals

The production and maintenance of *Meg1/Grb10* transgenic mice were reported in detail at elsewhere [31]. Transgenic (C57BL X C3H) F_2 mice were screened by PCR amplification of tail DNA samples using transgene-specific and endogenous Peg1 primer sets. Transgenic-positive founder mice (Meg1 Tg mouse) were backcrossed to C57BL/6NJcl (C57BL/6) mice, and the litters that were used in subsequent studies contained animals that were maintained within the C57BL/6 hybrid background. The Meg1 Tg mouse consists of 4 lines, with names of T10L, T18L, T20L, and T27L. We used these 4 lines for each experiment. Transgenic-negative mice were used as control mice. C57BL/6, NOD/ShiJcl (NOD), KK-A^y/TaJcl (KK-A^y), and BKS.Cg-+*Lepr*^{db}/+*Lepr*^{db}/Jcl (BKS) mice were also used in the RT-PCR experiment. Only male mice were used in our experiment.

This study was performed in accordance with the *Guidelines for Animal Experimentation of the National*

Institute of Infectious Diseases.

Body weight and body mass index (BMI)

Body weights of all mice used in our experiments were measured weekly from 4 weeks of age to 20 weeks. At 15 weeks of age, mouse length from nose to anus was recorded. Body mass index (BMI) was calculated as body weight (g) / body length^2 (cm).

Food and water intake

The mice were allowed free access to food pellets and water. We used either CMF (Oriental yeast Co., Ltd., Tokyo) or Quick Fat (CLEA Japan, Inc., Tokyo) for normal fat diet (NFD) and high fat diet (HFD), respectively. HFD contains high crude fat and glucose, which gives it a higher calorie count than NFD. Food intake per mouse was calculated as the average of 3 days intake at 11 weeks of age.

Organ weight

At 30 weeks of age 5 Meg1 Tg mice and control mice were sacrificed under deep ether anesthesia and necropsied. Visceral fat and livers were separated and weighed.

Glucose tolerance test and insulin tolerance test

Glucose tolerance tests and insulin tolerance test were performed on 11-week-old Meg1 Tg mice that had been fed on HFD. Glucose tolerance tests and insulin tolerance tests were performed after overnight fasting by administering glucose orally (2.0 g/kg body weight) and 0.3 μl of blood was collected from the tail vain after 0, 30, 60, and 120 min. The blood glucose level was measured by FreeStyle Meter (NIPRO, Osaka). Insulin tolerance tests were performed by an intraperitoneal injection of 1.0 U/kg of human insulin (Eli Lilly Japan, Tokyo) to Meg1 Tg mice and control mice; then 0.3 μl of blood was collected from the tail vein after 0, 30, 60, and 90 min. The blood glucose level was measured by FreeStyle Meter (NIPRO).

Plasma chemistry

Meg1 Tg and control mice were maintained on a normal light/dark cycle. Blood was collected from the mice with heparin at necropsy and inspection. The samples were centrifuged at 13,000 rpm centrifugation, and plasma was collected and stored at –30°C until assay. Plasma leptin, adiponectin, insulin and resistin were assayed by ELISA. Plasma total glucose, total cholesterol (TCHO), ammonia, triglyceride (TG), blood urea nitrogen (BUN), GOT, GPT, ALP, CPK, and LDH were measured using Fuji dry-chem 3000 (FUJIFILM Medical Co., Ltd., Tokyo). Livers and visceral adipose tissues were also recorded.

Histology

For histopathology, pancreas tissue samples were taken from Meg1 Tg and control mice at 20 weeks of age. The tissue samples were fixed in 10% buffer-neutralized formalin solution and embedded in paraffin. Sections were cut at 2 μm thickness and stained with hematoxylin and eosin.

Urinalysis and confirmation of the onset of 2DM

Urine collection was executed by compulsive urination at each weighing time, and urinary glucose was determined by Urolabostick (Biel-Sankyo Co., Ltd., Tokyo). When urinary glucose was detected, blood was collected from the tail vein. Confirmation of the onset of 2DM was decided by the detection of over 300 mg/ml of glucose in blood.

RT-PCR

Total RNA was extracted from livers, pancreata, skeletal muscles, and white and brown adipose tissues from 5 mice each of the Meg1 Tg, NOD, KK-A^y, BKS, and C57BL/6 strains of mice at 11 weeks of age, using the RNeasy system (QIAGEN K. K., Tokyo) according to the manufacturer's instructions. For the RT-PCR analysis, cDNA was synthesized from 1 μg of the total RNA using the SuperScript III First-Strand cDNA Synthesis System (Invitrogen Japan K. K., Tokyo) according to the manufacturer's instructions. The cDNA was PCR-amplified in 50 μl of reaction mixture containing 25 μl of TaqMan master mix (Applied Biosystems Japan Ltd., Tokyo) and 500 nM of the gene-specific (*Meg1/Grb10*, uncoupling protein 1 (*Ucp1*), glucose transporter 4 (*Glut4*), and *G3PDH* for normalization) TaqManProbe. The assays were performed in triplicate and the copy number of the *Meg1/Grb10*, *Ucp1*, and *Glut4* RNA were

calculated with an ABI Prism 7900 Sequence Detector (Applied Biosystems Japan). The data for each tissue were normalized to an internal standard (*G3PDH*).

Statistical analysis

Measurement data are shown as the mean value ± standard error (Mean ± SE). Statistical analysis of the data was performed using a one-factor ANOVA followed by Student's *t*-test. Comparison of the mean was calculated by Bonferroni's method. Covariance analysis was performed by Levene's method. Calculation of confidence limits and significance testing were made at a level of P=0.05.

Results

Postnatal growth curve

Fig. 1 shows the body weights of Meg1 Tg mice and controls that were fed either normal fat diet (NFD) or high fat diet (HFD). The weight of Meg1 Tg mice was normal until 4 weeks of age under both NFD and HFD diet conditions. However, their body weights did not increase as much as control mice after weaning and were 12 to 15% smaller than these of control mice at 20 weeks of age. These differences were statistically significant (P<0.05).

Food intake and BMI

For average food intake, no differences were observed between Meg1 Tg mice and controls under both diet conditions at 11 weeks of age (Fig. 2A: fed with HFD, 1.74 ± 0.02 g/day/10 g of body weight vs 1.65 ± 0.03 g/day/10 g of body weight; and with NFD, 1.65 ± 0.02 g/day/10 g of body weight vs 1.51 ± 0.07 g/day/10 g of body weight). However, BMI of Meg1 Tg mice were significantly lower than these of control mouse fed with HFD (P<0.05) both at 15 and 30 weeks of age (Fig. 2B: BMI at 15 weeks of age, 0.27 ± 0.01 g/cm^2 vs 0.32 ± 0.03 g/cm^2; and at 30 weeks of age, 0.29 ± 0.05 g/cm^2 vs 0.36 ± 0.07 g/cm^2).

Glucose tolerance test and insulin tolerance test

The plasma glucose level of Meg1 Tg mice fed with HFD at 11 weeks of age was significantly higher than those in both Meg1 Tg mice and controls fed with NFD

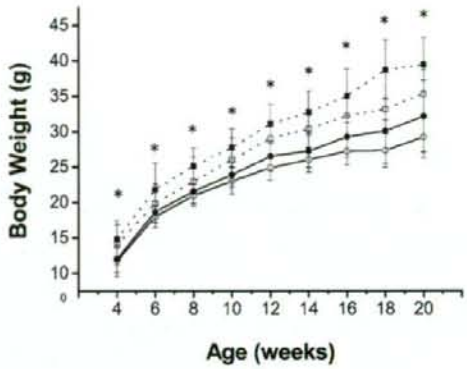

Fig. 1. Growth curve of control and Meg1 Tg mice from 4 to 20 weeks of age. Plotted values are means ± SE for 20 mice per group. Open square (□), control mice fed NFD; filled square (■), control mice fed HFD; open circle (○), Meg1 Tg mice fed NFD; filled circle (●), Meg1 Tg mice fed HFD. *P<0.05 (Student's t-test).

(P<0.05), indicating that their glucose tolerance was reduced (Fig. 3A). The reduction in blood glucose concentration after intraperitoneal administration of insulin was significantly delayed in Meg1 Tg mice compared to control mice fed with either HFD or NFD (P<0.05), indicating that Meg1 Tg mice had insulin resistance (Fig. 3B).

Organ weight

The weights of body, visceral fat, and liver, and the visceral fat/body weight ratios and liver/body weight ratios of Meg1 Tg and control mice at 10 to 12 weeks of age are shown in Table 1. The effect on organ weight by HFD feeding in Meg1 Tg mice was examined. When mice were fed HFD, weights of body, visceral fat and livers of Meg1 Tg mice were significantly lower than the controls (P<0.05), while liver/body weight ratio of Meg1 Tg mice was significantly higher than that of control mice (P<0.05). When Meg1 Tg mice were fed NFD, their body weight was significantly lower than the controls (P<0.05). There were no differences in visceral fat/body weight and liver/body weight ratios between Meg1 Tg and control mice irrespective of diet.

Plasma chemistry

The data on BUN, TG, insulin, adiponectin, resistin,

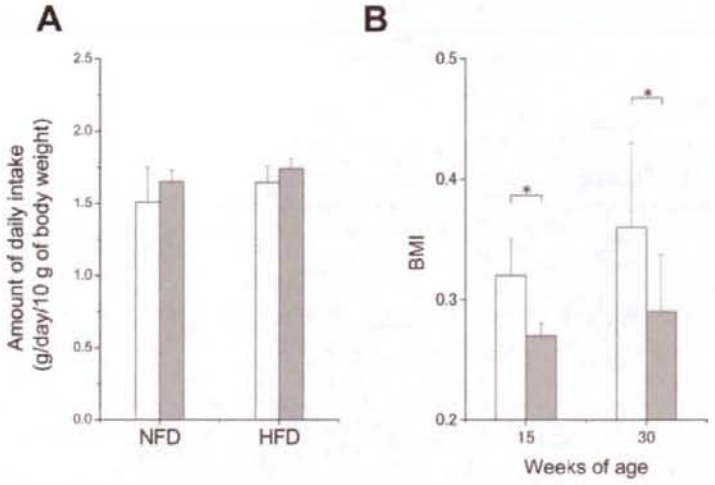

Fig. 2. Daily intake and BMI change in control and Meg1 Tg mice. (A) Daily intake of Meg1 Tg (▩) and control (□) mice at 11 weeks of age that were fed with NFD or HFD. There were no significant differences between the diet groups. (B) BMI of Meg1 Tg and control mice fed with HFD were calculated at 15 and 30 weeks of age. BMI of Meg1 Tg mice (▩) at both ages were significantly lower than those of control mice (□) ($P<0.05$).

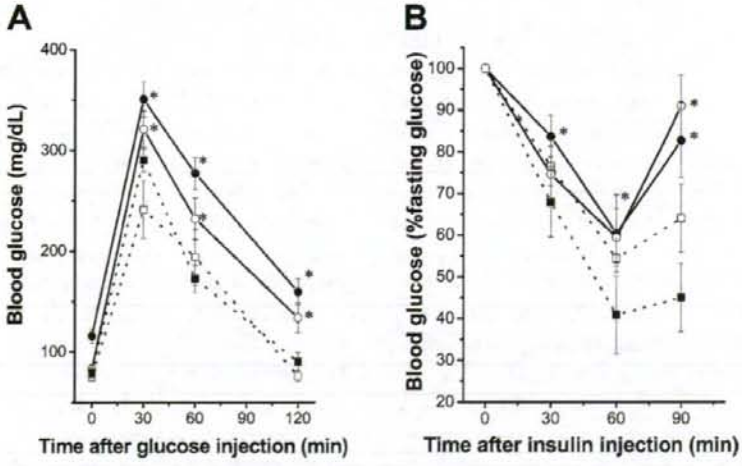

Fig. 3. Glucose and insulin tolerance level of Meg1 Tg and control mice. (A) Glucose tolerance in mice at 11 weeks of age that had been fasted overnight (n=10). (B) Insulin tolerance in mice at 11 weeks of age that had been fasted overnight (n=10). Plotted values are means ± SE for 10 mice per group. Open square (□), control mice fed NFD; filled square (■), control mice fed HFD; open circle (○), Meg1 Tg mice fed NFD; filled circle (●), Meg1 Tg mice fed HFD. *$P<0.05$ (Student's t-test). Glucose levels and their reduction rate in Meg1 Tg mice were significantly higher than in control mice.

Table 1. Liver, fat, and body weights of Meg1Tg and control mice at 10 to 12 weeks of age

	Control (NFD)	Meg1 Tg (NFD)	Control (HFD)	Meg1 Tg (HFD)
Body weight (g)	20.8 ± 0.6	18.4 ± 0.3[a)]	24.3 ± 0.3	19.6 ± 0.4[a)]
Visceral fat weight (mg)	197.6 ± 46.0	187.0 ± 68.6	507.5 ± 23.0	376.7 ± 29.6[a),b)]
Visceral fat/body weight ratio (mg/g)	9.0 ± 0.9	8.9 ± 1.6	18.8 ± 2.6	20.0 ± 1.1
Liver weight (mg)	900.2 ± 30	977.4 ± 38.5	1,001.0 ± 15.1	906.0 ± 41.8[a)]
Liver/body weight ratio (mg/g)	44.5 ± 3.7	51.6 ± 4.9	41.2 ± 1.3	44.9 ± 2.1[a)]

Values are the means ± SE for 10 mice per control and 10 mice per Meg1Tg. Meg1Tg (HFD) and control (HFD) mice were fed HFD. Meg1Tg (NFD) and control (NFD) mice were fed NFD. [a)]$P<0.05$ vs control, [b)]$P<0.05$ vs Meg1 Tg (NFD).

Table 2. Plasma chemistry in Meg1 Tg and control mice at 10 to 12 weeks of age

	Control (NFD)	Meg1 Tg (NFD)	Control (HFD)	Meg1 Tg (HFD)
BUN (mg/dl)	26.7 ± 1.9	20.6 ± 0.7	22.0 ± 0.8	19.3 ± 1.2[a)]
Triglyceride (mg/dl)	69.3 ± 23.2	90.6 ± 21.9	146.3 ± 11.4	202.0 ± 23.4[a),b)]
Insulin (pg/ml)	92.5 ± 13.4	153.3 ± 14.3	88.1 ± 16.9	152.4 ± 16.3[a)]
Adiponectin (ng/ml)	23 ± 4.01	46.8 ± 3.2	48.3 ± 7.0	74.4 ± 10.9[a),b)]
Resisitin (ng/ml)	2.28 ± 0.2	3.3 ± 0.2	3.6 ± 0.2	4.0 ± 0.2
IGF-1 (ng/ml)	395.8 ± 43.1	232.5 ± 28.3	358 ± 49.5	272.1 ± 24.4
Leptin (pg/ml)	548 ± 171	1,136.0 ± 267.0	1,036.0 ± 161.0	1,008.0 ± 146.0
NH3 (μg/dl)	143.1 ± 24.2	162.0 ± 12.2	223.1 ± 32.6	280.7 ± 50.9[b)]
Glucose (mg/dl)	161 ± 16.9	163.0 ± 12.6	172.8 ± 9.4	199.7 ± 58.4

Values are the means ± SE for 10 mice per control and 10 mice per Meg1Tg. Meg1Tg (HFD) and control (HFD) mice were fed bHFD. Meg1Tg (NFD) and control (NFD) mice were fed NFD. [a)]$P<0.05$ vs control, [b)]$P<0.05$ vs Meg1Tg(NFD).

IGF-1, leptin, ammonium, and glucose, measured at 10 to 12 weeks of age, are shown in Table 2. Irrespective of diet, plasma BUN in Meg1 Tg mice was significantly lower than in control mice ($P<0.05$). Plasma TG, insulin adiponectin and resistin in Meg1 Tg mice were significantly higher than in control mice ($P<0.05$), whereas plasma IGF-1 of Meg1 Tg mice tended to be lower than in controls. When mice were fed NFD, the plasma leptin concentration of Meg1 Tg mice was significantly higher than that of control mice. For, mice fed HFD, the plasma leptin level of Meg1 Tg mice was almost the same as the value of control mice (Table 2). Plasma glucose and ammonia in both NFD- and HFD-fed Meg1 Tg mice tended to be higher than those of control mice.

Other measured biochemical markers such as TCHO, GOT, GPT, ALP, CPK, and LDH plasma concentrations measured in Meg1 Tg and control mice of the same age were almost similar (data not shown).

Histological analysis

We found two histological abnormalities in the pancreatic tissues of Meg1 Tg mice fed NFD: atrophy of the pancreatic acinus cells and an increase in adipocytes at 20 weeks of age; and enlargement of islet of Langerhans (Fig. 4B). When Meg1 Tg mice were fed HFD, the above-noted pathological abnormalities were more severe than these of NFD feeding (Fig. 4C). Pathological abnormalities did not develop in control mice fed NFD or HFD (Fig. 4A).

The onset rate of type 2 diabetes

The onset rates of 2DM between Meg1 Tg mouse fed NFD and HFD at 25 weeks were 11.3% and 60.0%, respectively (Fig. 5A). This clearly demonstrates that feeding with HFD induces 2DM in Meg1 Tg mice. There were no symptoms of 2DM in control mice up to 30 weeks of age.

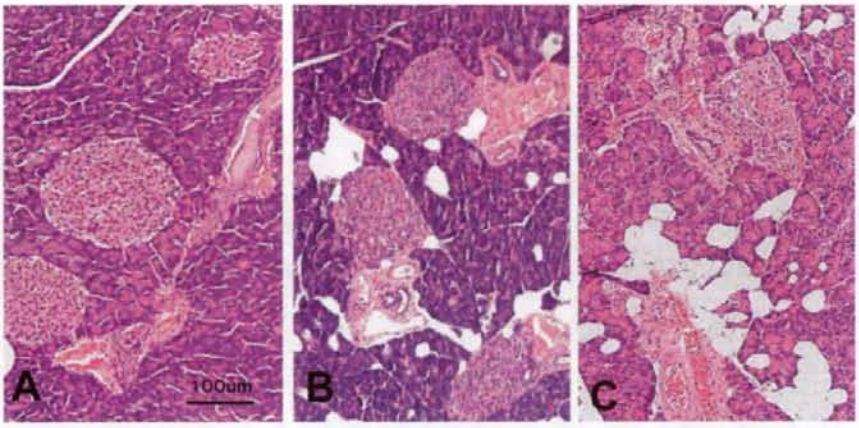

Fig. 4. Light microscopic features of pancreata from control and Meg1 Tg mice around 20 weeks of age. Heamatoxylin and eosin stain, × 100. (A) Control mouse. (B) Meg1 Tg mouse fed NFD. (C) Meg1 Tg mouse fed HFD. Vacuolation and denaturation at exocrine pancreas in the Meg1 Tg mouse was found. Furthermore, enlargement of an islet of Langerhans was observed. The pathological abnormality of Meg1 Tg mice fed HFD was more severe than that of NFD-fed Meg1 Tg mice.

Meg1/Grb10, Ucp1, *and* Glut4 *expression in Meg1 Tg and 3 diabetes model mice*

For further analytical research, we examined diabetes related gene expressions of Meg1 Tg mice in comparison with NOD, KK-A^y, BKS, and C57BL/6 mice. *Meg1/Grb10*, *Ucp1*, and *Glut4* expression ratios against control gene are shown in Fig. 6. *Meg1/Grb10* gene expression of skeletal muscle of Meg1 Tg mice was 100 times higher than those of the other 3 diabetes model mice and the C57BL/6 mouse (Fig. 6A: $P<0.05$). In contrast, *Glut4* expression of skeletal muscle of Meg1 Tg mice was significantly lower than these of the 3 diabetes model mice and the C57BL/6 mouse (Fig. 6C: $P<0.05$). There were no differences of *Ucp1* gene expression in brown adipose tissue between Meg1 Tg and the 3 diabetes model mice and the C57BL/6 mouse. Meg1 Tg mice fed HFD showed suppression of *Ucp1* gene expression in brown adipose tissue (Fig. 6).

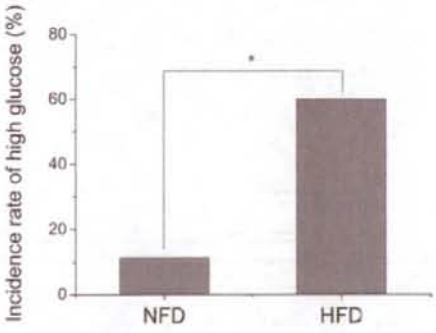

Fig. 5. Increased incidence rate of high blood glucose in Meg1 Tg mice fed HDF. Meg1 Tg mice were fed NFD and HFD for 25 weeks. The onset rates (■) of type 2 diabetes, the decided by the detection of over 300 mg/ml of glucose in the blood, in the Meg1 Tg mouse were compared by diet. HFD feeding-induced diabetes was significantly higher than NFD feeding. *$P<0.05$ (Student's t-test).

Discussion

We evaluated the Meg1 Tg mouse as a non-obese 2DM animal model in this study. Two of the major defects seen in 2DM are insulin resistance of targets, such as liver, muscle and adipose tissues, and impaired insulin secretion from pancreatic β-cells [26, 37, 38]. Histological analysis revealed the pancreatic abnormality in Meg1 Tg mice (Fig. 4). Moreover, Meg1 Tg mice showed both the insulin resistance and glucose intoler-